



# OPEN Failure analysis of 3Cr oil pipe body fracture

Jinzhong Wang<sup>1✉</sup>, Yan Li<sup>2</sup>, Xianren Kuang<sup>1</sup>, Yaqin Ma<sup>2</sup>, Jinheng Luo<sup>1</sup> & Yan Long<sup>1</sup>

With the green and low-carbon development of oilfield, more and more repaired oil tube is used as oil and gas transportation pipeline, but there is a difference between the manufacturing and repairing standard of oil tube, and some problems inevitably occur in the use process. In this paper, we studied a 3Cr repaired oil tube body fracture accident that occurred in an oilfield oil and gas well. In order to determine the reason for the repaired oil tube fracture, macro-morphological analysis, magnetic particle detection, chemical composition analysis, mechanical properties analysis, metallographic analysis, scanning electron microscopy (SEM), energy spectrum analysis and corrosion product XRD analysis were used to analyze the repaired oil tube body. The results indicate that the tensile strength, yield strength, Rockwell hardness and chemical composition of the repaired oil tube material meet the requirements of the technical agreement for 3Cr low alloy steel, and the metallographic organization of the failed oil tube material is tempered sorbite, and its organizational grain size is 9.0 grade. The natural gas injected by gas lift contains oxygen and trace hydrogen sulfide, and the formation water is calcium chloride water type, which together form a high stress corrosion cracking sensitivity environment. In addition, corrosion pits and stress corrosion cracks are generated in the service process of the oil tube, which makes the bearing capacity of the oil tube decrease, and plastic fracture of the oil tube occurs under large axial load.

**Keywords** 3Cr, Repaired tube, Oil tube break, Stress corrosion

Oil and gas are one of the major energy resources in the world, supporting the economic development of each country<sup>1</sup>. Oil tube plays an important role in the process of oil and gas extraction. With the increasing demand for energy in production development, the environment of oil and gas wells is gradually harsh. The increasing water content of oil wells, even more than 90%<sup>2</sup>, and the method of oil wells extraction has also changed, and the traditional injection of water<sup>3</sup> or gas is changed to the injection of CO<sub>2</sub><sup>4–6</sup> and polymer injection, and so on. As a result, the environment in which oil tubing and casing are used has become progressively harsher. As the exploitation environment becomes more and more severe and the amount of oil-extracted increases every year, the failure of oil tubes is becoming more and more serious. During the inspection process of used oil tubes, some oil tubes may be replaced. Moreover, the replaced oil tube will be reused after the used oil tube is inspected and repaired in order to reduce the waste and realize the green and low-carbon production in China. Oil and gas mixtures extracted from oilfields often contain formation water, various types of salt and corrosive components such as H<sub>2</sub>S and CO<sub>2</sub><sup>7–22</sup>. The inner wall of the oil tube will be affected by corrosion, perforation, wall thickness thinning and even oil tube fracture<sup>23–28</sup>. Oil tube is the lifeline of oil and gas extraction, once the corrosion fracture occurs. Due to pipeline corrosion, there are many major problems in the process of oil and gas field development, which not only pose a great threat to the safe operation of oil and gas fields, but also cause huge economic losses<sup>29–34</sup>. Therefore, it is necessary to accurately analyze the causes of corrosion fracture of oil tube and propose targeted preventive measures to reduce the occurrence of similar accidents. In this study, the cracking failure of repaired oil tube as a continued use of oil tube was investigated. Such failure cases are less frequently reported, so these findings are important references for the application of repaired oil tubes.

## Incident overview

The fractured tube is a Φ73.02 mm×5.51 mm 110-3Cr EU repaired tube, which was re-entered into the well in September 2020, and the fracture of the tubing column occurred from January 2024 onwards, as shown in Fig. 1.

The oil and gas wells where the fractured tubing was located were drilled on July 27th, 2011, and completed on September 23rd, 2011, with a drilling depth of 5860 m. the well was completed by perforating on October 5th, 2011. The well was tested and connected on October 8th, 2011. The well was delivered on November 2nd, 2011,

<sup>1</sup>Tubular Goods Research Institute, China National Petroleum Corporation & State Key Laboratory of Service Behavior and Structural Safety of Petroleum Pipe and Equipment Materials, Xi'an 710077, China. <sup>2</sup>Tarim Oilfield Company, PetroChina, Co., Ltd., Korla 841000, China. ✉email: swawjz@qq.com



Fig. 1. 3Cr oil tube.

Formation water					
Geology	Sampling date	Chloride ion (mg/L)	Total mineralization (mg/L)	Hydroentanglement	PH
C	2019-11-01	100,000	164,300	CaCl <sub>2</sub>	6.30
Crude oil					
Geology	Sampling date	20℃ density (g/cm <sup>3</sup> )	50℃ density (g/cm <sup>3</sup> )	Dynamic viscosity (mPa·s)	Deposit (%)
C	2020-01-02	0.8649	0.8441	7.120	0.07
Asphaltene (%)	Colloid (%)	Sulfur content (%)	Wax content (%)	Freezing point (℃)	/
9.37	1.22	0.510	9.800	−2.00	/
Natural gas					
Geology	Sampling date	O <sub>2</sub> , % (mol/mol)	CO <sub>2</sub> , % (mol/mol)	H <sub>2</sub> S, % (mol/mol)	N <sub>2</sub> , % (mol/mol)
C	2020-01-03	0.9883	0.0210	0.0000	72.48

Table 1. Well formation water, crude oil and natural gas fractions.

with a top of 5756 m and a bottom of 5808 m. the well deviation data are as follows: the well depth is 5831.6 m, the azimuth is 315.92 °, and the inclination is 2.52 °. The completion fluid is organic salt with a density of 1.08 g/cm<sup>3</sup>. The well was converted to gas lift operation on August 29th, 2020 and completed on September 19th, 2020. From October 2020 to December 2022, the well is mainly produced by natural gas lift; On December 23rd, 2022, it was converted to flowing production, and then shut in due to high gas oil ratio. See Table 1 for the fluid composition analysis data of the well.

Test methods and results  
Macro-morphological analysis

The macroscopic morphology of the fractured oil tube is shown in Fig. 2. The outer surface of the oil tube is black, with no obvious corrosion products, and there is a certain degree of necking at the fracture. The inner surface is rusty yellow, with a large number of corrosion products that can be easily dislodged. There are a large number of corrosion pits on the inner surface of the oil tube. The fracture is mainly divided into two districts, the source area and the extension area, and the extension area mainly consists of the shear lip, accounting for more than 80%. The corrosion pits mainly have a rounded blunt shape morphology, as shown in the 3D measurements of Fig. 3. The depth of the corrosion pits is about 0.287 ~ 0.785 mm, and the average annual corrosion rate is 0.086 ~ 0.236 mm/a, as shown in Table 2.

Geometric measurement

Vernier calipers and thickness gauge were used to measure the geometric dimensions of the fractured tube, the specific locations of the measurement points are shown in Fig. 4, and the measurement results are shown in Table 3. It can be found that the measured values of the outer diameter and wall thickness of the oil tube body did not show significant changes, while the breakage of the oil tube has been characterized by an obvious necking.

Non-destructive testing

According to ASTM E 709 – 14 standard, magnetic particle inspection was carried out on the inner and outer surfaces of the fractured oil tube with the help of ZCM-DA1206A magnetic particle flaw detector, as shown in Fig. 5 ~ Figure 6. As can be seen from the test results, no crack characteristics were found on the outer surface of the fractured oil tube, and a total of 6 cracks were found on the inner surface.

Chemical composition analysis

The chemical composition analysis specimen is taken from the oil tube fracture and the body, and according to GB/T 4336 – 2016 standard, the ARL 4460 direct reading spectrometer is used to analyze the specimen chemically, and the results are shown in Table 4. The test results show that the chemical composition of the oil tube meets the requirements of the technical agreement for the 3Cr material.

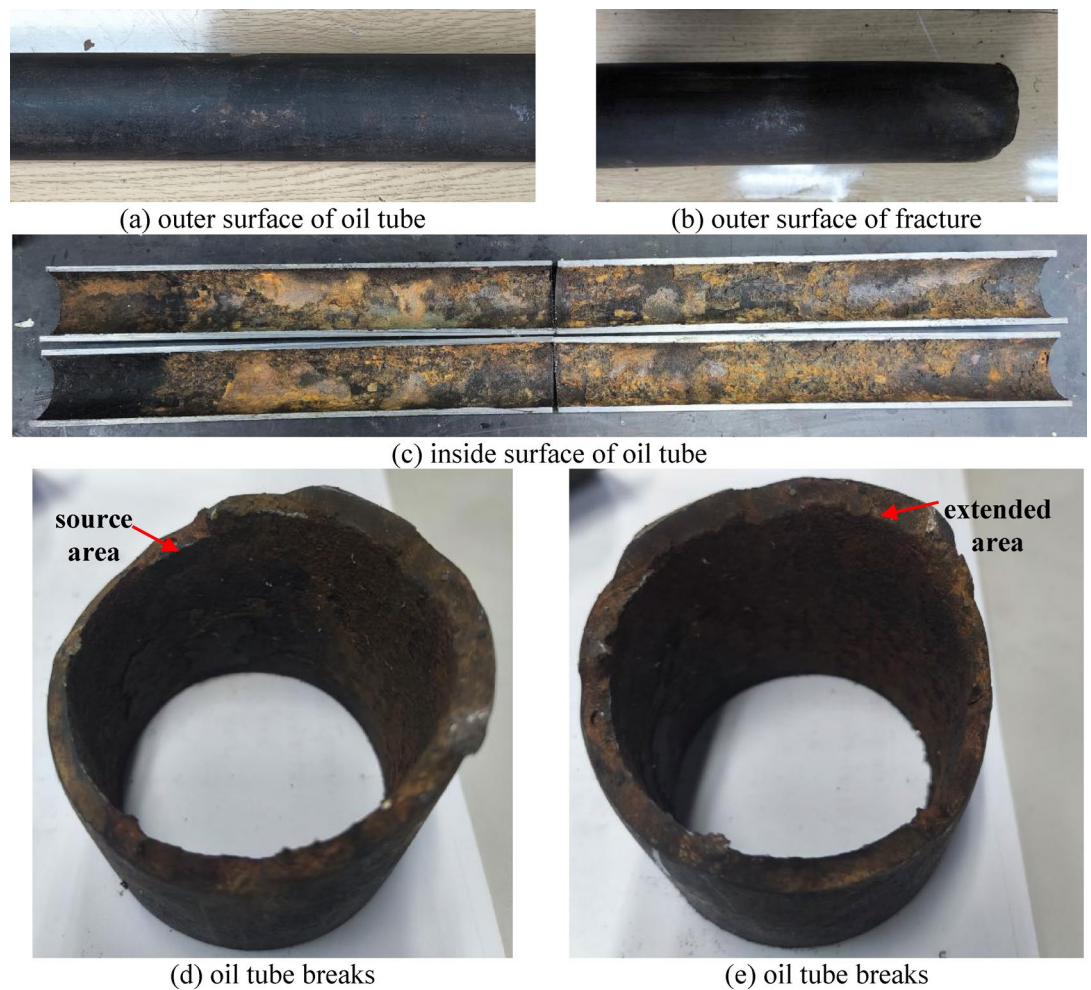


**Fig. 2.** Macroscopic shape of oil tube.

### Mechanical properties analysis

Longitudinal tensile specimens were taken from the fracture and the body of the fractured oil tube, and room temperature tensile test was carried out with the help of UTM 5305 material testing machine according to the ISO 6892-1:2019 standard, and the results are shown in Table 5. Transverse and longitudinal hardness specimens were taken from the fracture and the body of the fractured oil tube, respectively, and Rockwell hardness test was carried out with the help of RB 2002T Rockwell hardness tester according to the GB/T 230.1–2018 standard, and the results are shown in Table 6. The results of the mechanical properties test show the tensile strength, yield strength, and Rockwell hardness of the fractured oil tube body meet the requirements of the technical agreement for 3Cr material, while 66.7% of the specimens of fractured oil tube after break elongation do not meet the requirements of the technical agreement for 3Cr material.

### Metallographic analysis

According to ASTM E45-18a, GB/T 13,298–2015 and GB/T 4335–2013 standards, the microstructure, grain size and non-metallic inclusions were analyzed by MEF4M metallographic microscope, OLS 4100 laser confocal microscope and image analysis system. The analysis results are shown in Table 7, and the microstructure photos are shown in Fig. 7. The grade of non-metallic inclusions at the fracture and body of the oil tube is A0.5 and D0.5, the microstructure is tempered austenite, the grain size is 9.0, and there is no obvious microstructure abnormality. Metallographic cross-section samples were taken from the typical crack area on the inner surface of the oil tube for analysis, and the results were shown in Fig. 8. It can be seen that the crack originated from the corrosion pit on the inner surface of the oil tube, and there was no abnormal surrounding tissue in the corrosion pit area. The overall bifurcation of the crack was less, and there was no abnormal surrounding tissue.

### Micro-analysis

#### *Corrosion pit analysis*

The samples were randomly taken from the internal corrosion area of the fractured oil tube, and the microstructure observation and energy spectrum analysis of the samples were carried out by scanning electron microscope and its accompanying energy spectrum analyzer. From Fig. 9, it can be seen that there are many corrosion pits on the

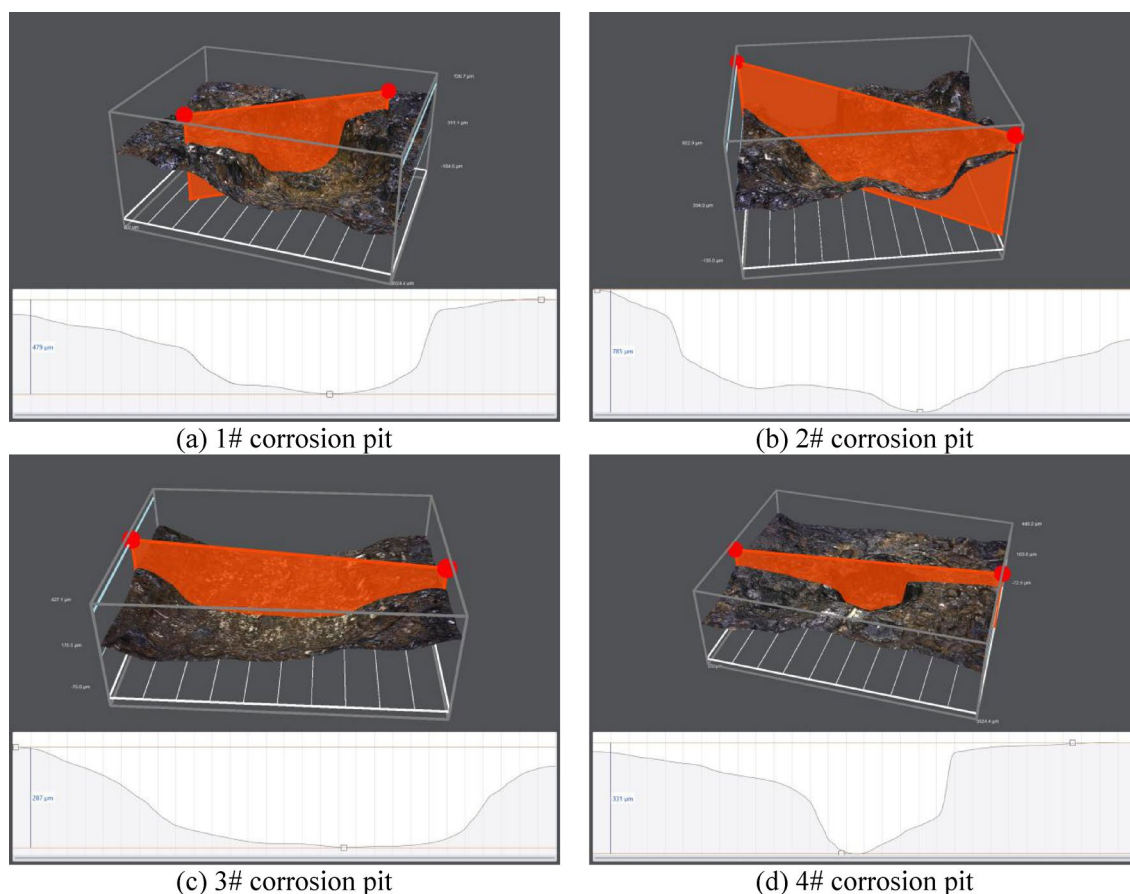


**Fig. 3.** 3D measurement results of corrosion pits on the inner surface.

Corrosion pit location	Corrosion pit depth (mm)	Pitting corrosion rate (mm/a)
1# corrosion pit	0.479	0.144
2# corrosion pit	0.785	0.236
3# corrosion pit	0.287	0.086
4# corrosion pit	0.331	0.099

**Table 2.** Oil tube corrosion pit depth measurements and pitting corrosion rates (oil tube downhole in September 2020, dumping from January 2024, total 3.33 years).



**Fig. 4.** Schematic diagram of geometric dimension measurement points.

inner surface of the oil tube, and there are a large number of dense corrosion products in the corrosion pit area. The cracking characteristics of the substrate surface can be observed at high magnification. Figure 10 shows the energy spectrum analysis results of the selected partial corrosion zone. There are high contents of O, Fe, S, Cl, Cr and other elements on the inner surface of the fractured oil tube.



Measurement area	Outer diameter (mm)		Wall thickness (mm)				
	Measurement results 1	Measurement results 2	0°	90°	180°	270°	average value
Pipe end (A)	73.60	73.60	5.55	5.47	5.06	5.59	5.42
Central section (B)	73.66	73.62	5.55	5.76	5.43	5.42	5.54
Breakage (C)	71.71	72.06	4.82	4.99	4.95	5.14	4.98
Technical agreement on 3Cr requirements	72.23 mm ~ 73.81 mm		≥ 4.82 mm				

**Table 3.** Geometric measurement results.



**Fig. 5.** Oil tube outer surface inspection results.

#### Fracture surface analysis

Samples were taken from the source area and the expansion area of the fractured oil tube. After cleaning by ultrasonic + alcohol cleaning + cellulose acetate adhesive method, the fracture samples were observed by TESCAN VAGE II scanning electron microscope analysis system for microscopic morphology observation and X-ray energy spectrum analysis. The results are as follow:

The results of the oil tube section morphology and energy spectrum analysis are shown in Figs. 11, 12 and 13. From Fig. 11, it can be seen that the micro-morphology of the source area of the cross-section is blocky, with obvious traces of cracking and the presence of a large number of corrosion products. The extended area of the section shows some tiny wineglass-shaped microporous pits, also called the tough nests. The tough nest is the trace left on the fracture surface after the material plastic deformation in the micro-area range of the microvoid produced by the nucleation, growth, aggregation, and finally interconnected and led to fracture. The results of the energy spectrum analysis show that the S and Cl contents in the fracture source area are higher than those in the fracture extension area, while in terms of the Cr content, the concentration in the source area is 10.45%, which is much higher than the 3% in the 3Cr steel matrix. This is mainly related to the corrosion resistance mechanism. In the initial stage of corrosion, Cr will dissolve rapidly and accelerate the material corrosion due to its higher activity than Fe. However, when the  $\text{Cr}^{3+}$  produced by dissolution precipitates to form  $\text{Cr}(\text{OH})_3$  and mixes with the corrosion products, a Cr-rich product film is formed, and this dense Cr-rich layer hinders further dissolution of the metal, thus reducing the corrosion rate of the material.

#### Crack analysis

Two samples were selected from the cracks found in the magnetic particle testing of the inner surface of the fractured tubing, and the scanning electron microscope and its attached energy spectrum analyzer were used to observe the microstructure and analyze the energy spectrum of the samples. The crack mainly originated from the bottom of the corrosion pit on the inner surface of the oil pipe. As shown in Fig. 14, the crack propagated along the wall thickness direction, and there were a large number of corrosion products in the crack. The crack initiation position has obvious morphological characteristics, showing a round blunt shape, which is consistent with the shape of the corrosion pit, indicating that the crack is gradually developed on the basis of the corrosion pit. The results of energy spectrum analysis show that the distribution characteristics of crack elements are similar, mainly including Fe, O, Cr, Cl and other elements, as shown in Figs. 15 and 16 (the regions in the figure are root, middle and tip from top to bottom in turn).

#### XRD analysis of corrosion products

Attachments were removed mechanically from different locations on the inner surface of the oil tube, and an X-ray diffraction analyzer (XRD) was applied to analyze the physical phase of the corrosion products, as shown in Fig. 17. The results show that the main corrosion products on the inner surface of the oil tube are iron oxide

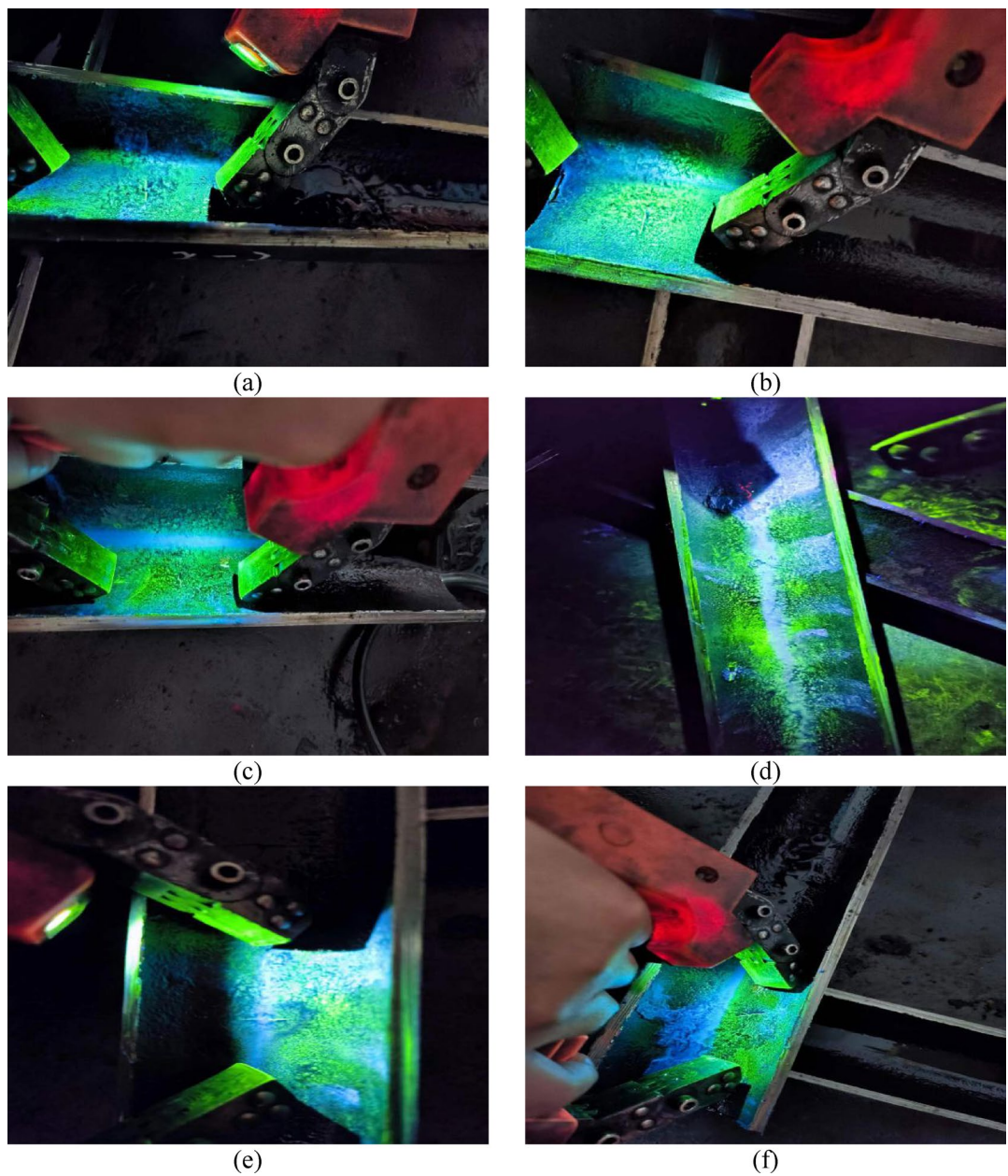


**Fig. 6.** Oil tube inner surface inspection results.

Element Specimen	C	Si	Mn	P	S	Cr	Mo	Nb	V	Ti	Cu
Fracture transverse	0.20	0.33	0.51	0.0091	0.0012	3.03	0.39	0.0021	0.012	0.017	0.23
Fracture longitudinal	0.19	0.33	0.52	0.0085	<0.001	2.93	0.39	0.0021	0.013	0.018	0.22
Tube body transverse	0.20	0.32	0.51	0.0090	0.0013	3.04	0.39	0.0028	0.013	0.018	0.23
Tube body longitudinal	0.20	0.33	0.52	0.0089	0.0012	2.97	0.39	0.0021	0.013	0.018	0.23
Technical agreement on 3Cr requirements	/	/	/	≤ 0.015	≤ 0.010	/	/	/	/	/	/

**Table 4.** Chemical composition analysis results (wt%).

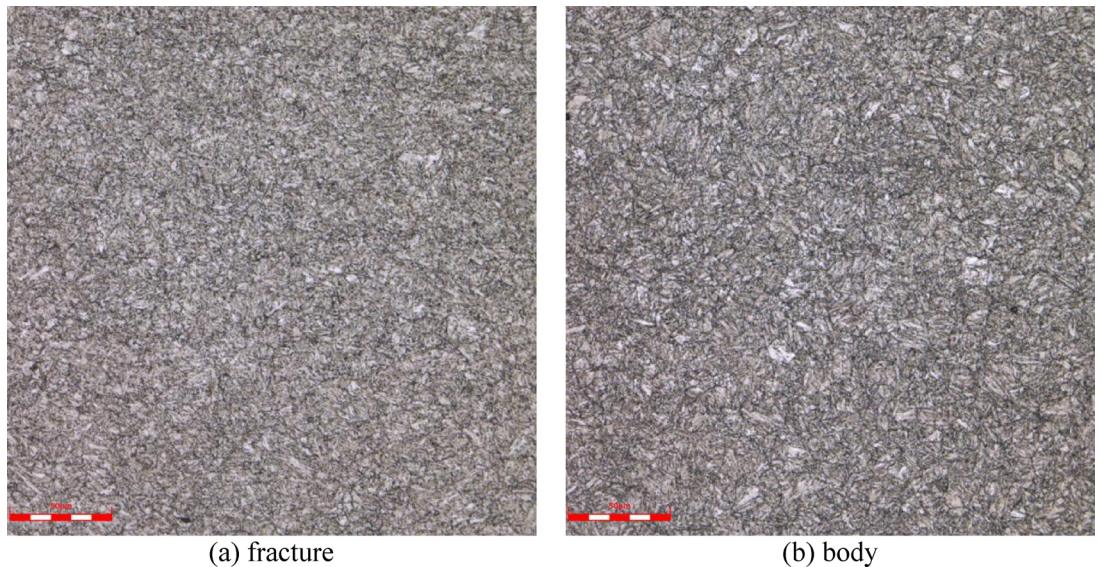
Specimen		Tensile strength	Yield strength (0.6%EUL)	Post-break elongation
Serial number	Diameter/width×marking distance (mm)	(MPa)	(MPa)	(%)
Fracture	19.1 × 50	930	850	15.5
		924	873	13.0
		931	865	18.0
Body	19.1 × 50	928	841	15.0
		920	838	17.0
		904	822	14.5
Technical agreement on 3Cr requirements	/	≥ 793	758–965	≥ 16

**Table 5.** Tensile strength test results.

Serial number	Inspection area	HRC
Fracture	Transverse	29.0, 29.3, 29.6
	Longitudinal	29.0, 28.7, 28.5
Body	Transverse	28.2, 28.9, 28.9
	Longitudinal	29.5, 29.6, 29.7
Technical agreement on 3Cr requirements		≤ 32

**Table 6.** Rockwell hardness test results.

Specimen	Non-metallic inclusions								Microstructure	Grain size
	A		B		C		D			
	Thin	Thick	Thin	Thick	Thin	Thick	Thin	Thick		
Fracture	0.5	0	0	0	0	0	0.5	0	Tempered austenite (Fig. 7a)	9.0
Body	0.5	0	0	0	0	0	0.5	0	Tempered austenite (Fig. 7b)	9.0

**Table 7.** Metallographic analysis results.**Fig. 7.** Microstructure photos of fractured tube.



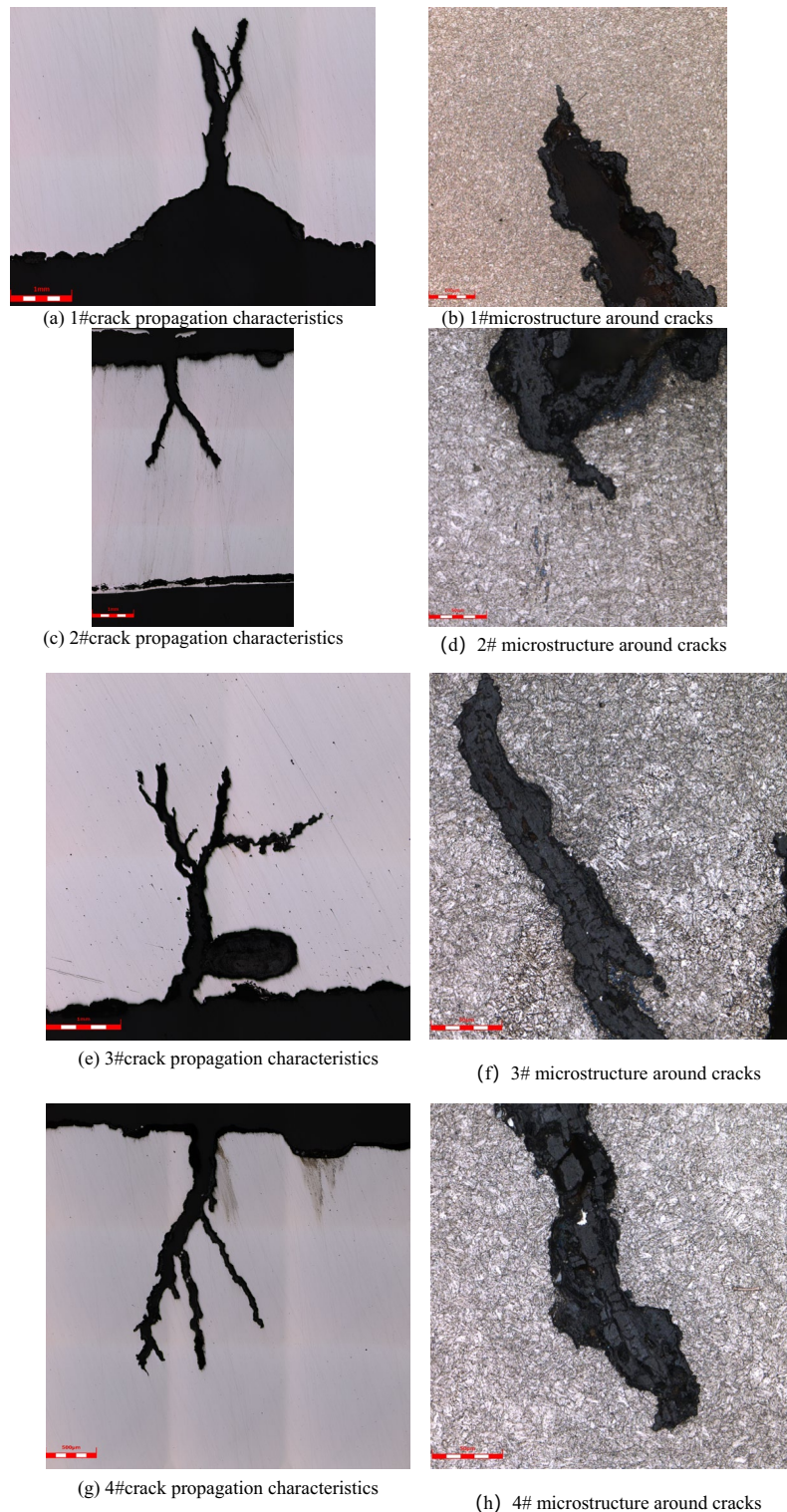


**Fig. 8.** Metallographic section characteristics of oil tube crack.

phase ferric oxide ( $\text{Fe}_2\text{O}_3$ ), followed by ferrous carbonate ( $\text{FeCO}_3$ ), ferrous chloride ( $\text{FeCl}_2$ ) and ferrous sulfide ( $\text{FeS}$ ).

### Comprehensive analysis

The above physical and chemical test results of the oil tube material show that the tensile strength, yield strength, Rockwell hardness and chemical composition of the oil tube material are in line with the requirements of the technical agreement for 3Cr low alloy steel. The metallographic organization of the oil tube is tempered austenite,



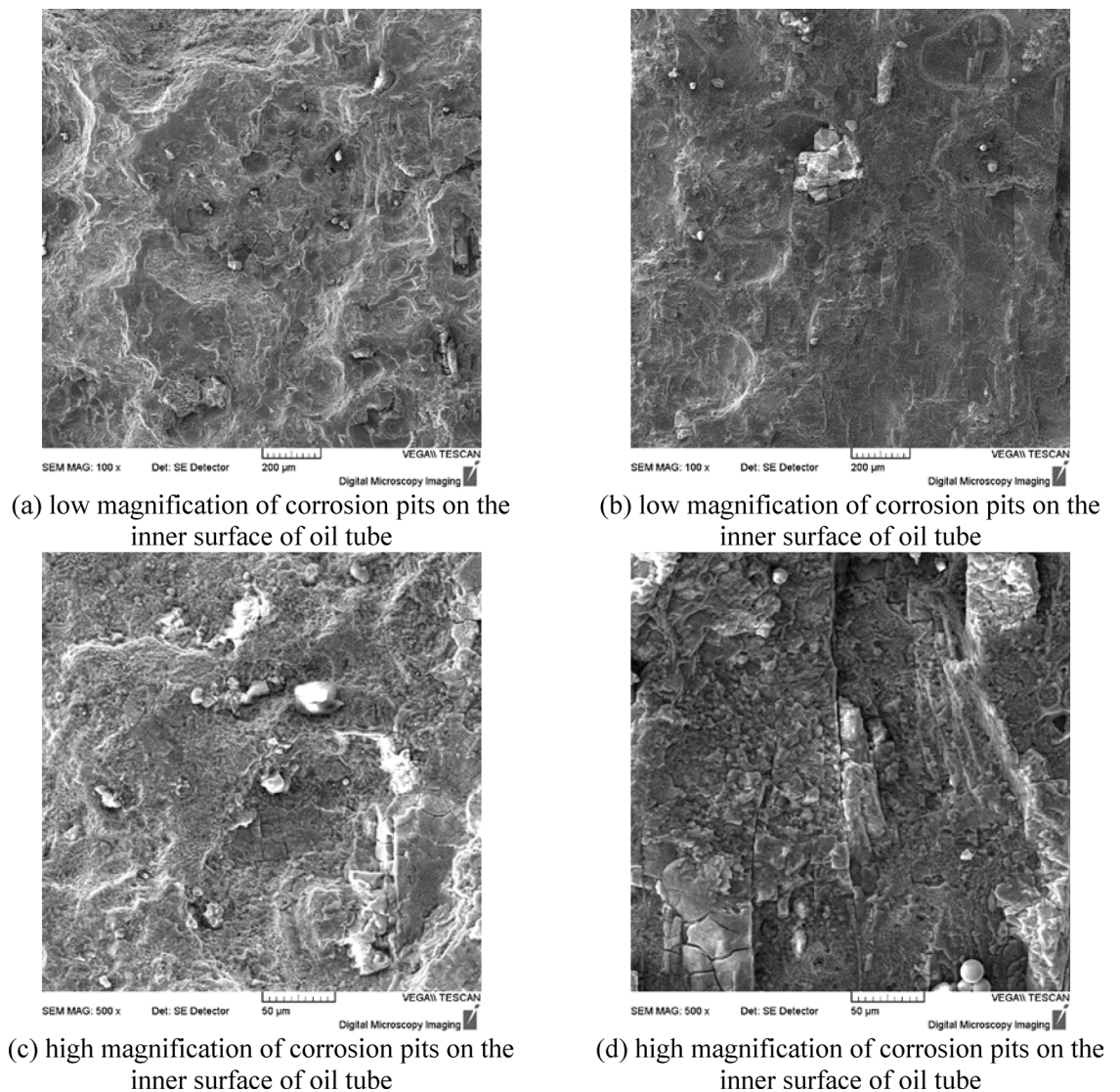


**Fig. 9.** Micro-morphology of corrosion pits on the inner surface of oil tube.

grain size grade 9.0, the sum of the four types of non-metallic inclusions grade does not exceed 2.0, the oil tube material metallographic organization is not abnormal. The microstructure analysis showed that although 3Cr steel had good corrosion resistance, it still showed high stress corrosion sensitivity in the complex environment containing oxygen and  $\text{Cl}^-$ . The reasons for the fracture of oil tube are analyzed by combining the morphological characteristics of the fracture of oil tube and the well service condition of oil tube.

Macroscopic observation and analysis of fracture surface and metallographic analysis of crack section show that the fracture tubing section is composed of source area and propagation area. The source area is flat and dark, and originates from the bottom of corrosion pits on the inner wall of tubing, which is similar to the failure position of heat exchanger described in document<sup>35</sup>. The surface of these corrosion pits presents honeycomb morphology, which is a typical feature of chloride ion corrosion. There are bifurcations at the crack tip, and a large number of small secondary cracks are distributed on both sides of the main crack. These secondary cracks are at an angle of  $45\text{--}60^\circ$  with the main crack, reflecting that the stress corrosion crack is affected by multidirectional stress in the process of propagation, which conforms to the characteristics of sulfide stress cracking described in document<sup>36</sup>. In addition, the fracture has obvious necking (belonging to plastic fracture), and the shear lip of the section accounts for a large proportion, indicating that the tubing bears a large axial tensile load during service.

Microscopic observation of the crack growth zone by scanning electron microscope (SEM) showed that the main crack showed typical transgranular growth characteristics, and the crack path was tortuous with obvious secondary crack branches. The internal morphology of the crack shows that the wall presents a typical “muddy crack” feature, and the surface is covered with a loose corrosion product layer, which is in sharp contrast to the smooth section of conventional mechanical fracture. Irregular serrated edges can be observed in the crack tip region, indicating that the crack growth process is accompanied by a continuous anodic dissolution process.

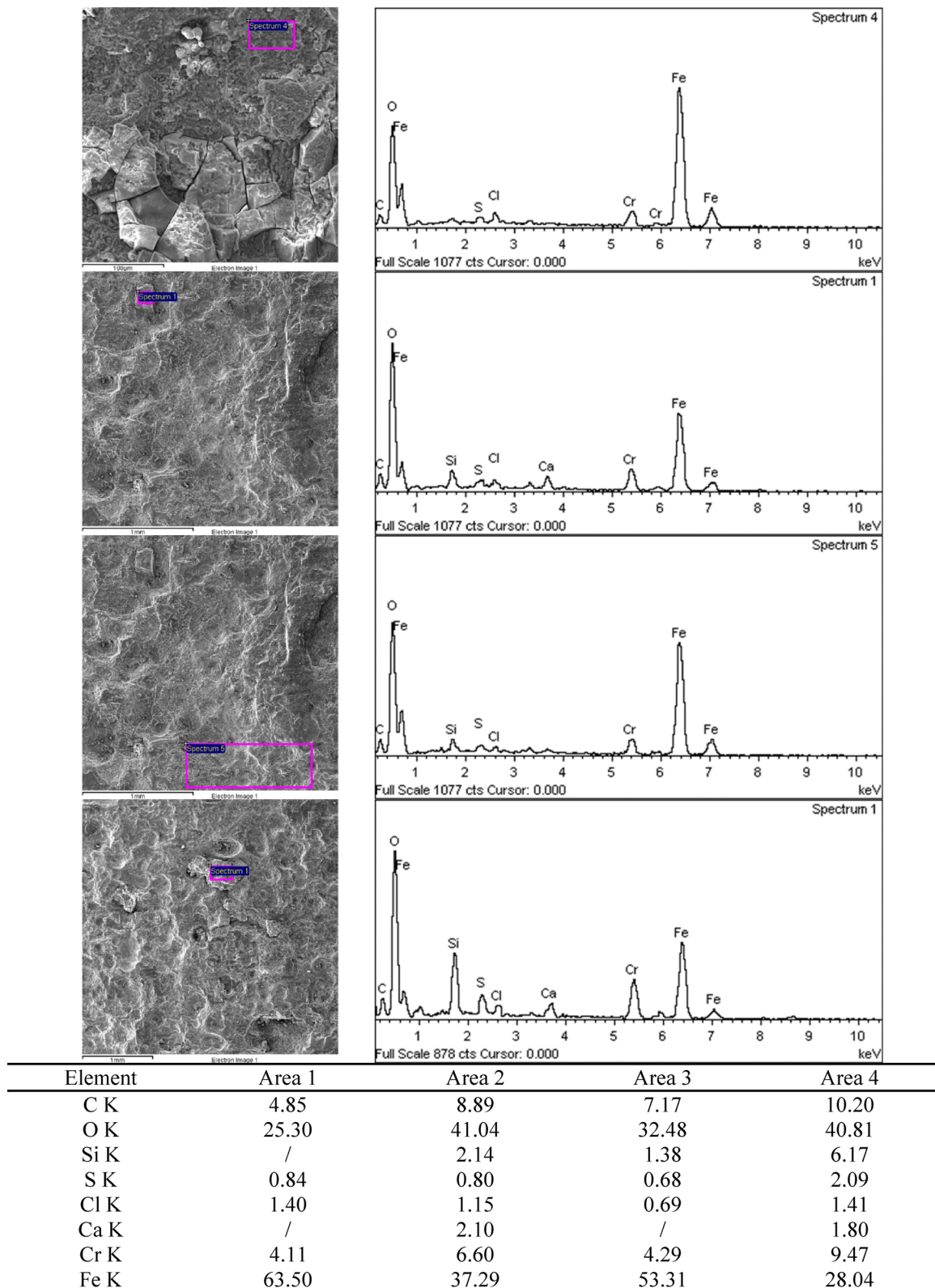


**Fig. 10.** The energy spectrum analysis results of corrosion pits on the inner surface of the oil tube.

The energy spectrum analysis showed that the content of Cl in the crack was significantly higher than that in the matrix area, and an obvious Cl enrichment zone was formed at the crack tip, which confirmed the key role of  $\text{Cl}^-$  in the stress corrosion process. There is a corrosion affected zone on both sides of the crack, in which the abnormal Fe/O atomic ratio is detected by energy spectrum, indicating the selective dissolution of iron.



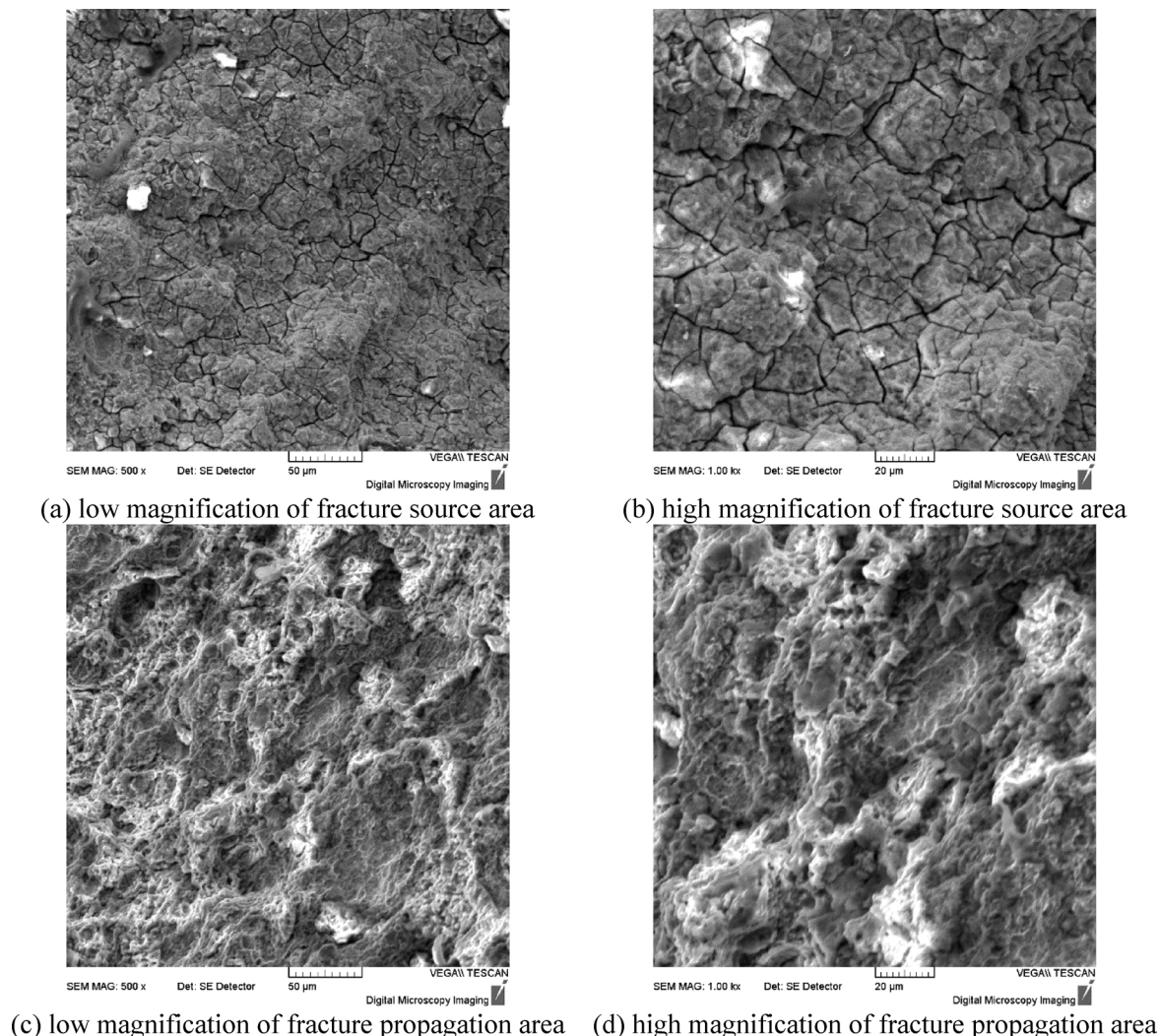


**Fig. 11.** Micromorphology of oil tube fracture.

The results of energy spectrum analysis show that the material in the fracture, crack and corrosion pit inside the oil tube mainly contains the elements of O, Fe, Cr, Cl and S. Fe and Cr are the matrix elements of the oil tube, and the elements of O, Cl and S are imported from the outside world. The medium in the well shows that the formation water is  $\text{CaCl}_2$  type, and the  $\text{Cl}^-$  content is 100,000 mg/L. It can be determined that the Cl in the fracture, cracks, and corrosion pits on the inner surface of the oil tube originates from the formation water. The produced natural gas of the well does not contain  $\text{H}_2\text{S}$  gas, but the well is gas-lifted production of natural gas, and the produced gas of the gas-lifted gas source well is detected to contain trace amounts of  $\text{H}_2\text{S}$  gas, as shown in Table 8. Since the 3Cr oil tube is very sensitive to  $\text{H}_2\text{S}$ , certain corrosion products would be produced, but due to the extremely low content of  $\text{H}_2\text{S}$ , there is a small amount of S in the corrosion products. The  $\text{O}_2$  content of the natural gas produced from this well is 0.9883%(mol/mol), and the  $\text{O}_2$  content of the natural gas produced from the gas source well is 1.598%(mol/mol). In addition, through communication with the field technicians, it is confirmed that when the gas source well is insufficient, the gas from the surplus gas station is used as the gas source for this well. In addition, through communication with the field technicians, it was confirmed that when the gas source wells were short of gas, the gas from the “surplus gas station” was used as the gas source for the wells. As single wells are commonly used to induce spraying through annular nitrogen gas lift, continuous tubing + nitrogen truck gas lift to remove acid residue, annular nitrogen gas lift to remove liquid, and continuous tubing + nitrogen truck gas lift to produce, and so on. The oxygen contained in the nitrogen would enter the surplus station and the joint station along with the produced natural gas. Oxygen would not be consumed in the surface system, which would bring oxygen corrosion problems to underground pipes and columns when it is used as a source of gas lift gas.

Oxygen dissolved in water is seriously corrosive to steel, but does not directly cause stress corrosion cracking. Combined with the results of energy spectrum analysis, it is believed that oxygen corrosion occurred in the oil tube, and chloride stress corrosion cracking occurred under the action of  $\text{Cl}^-$  ions. Usually, the mechanism of chloride stress corrosion generation includes three aspects. First, chloride in the medium can increase the metal stress concentration degree, making the metal surface appear tiny stress concentration area. Secondly, chloride

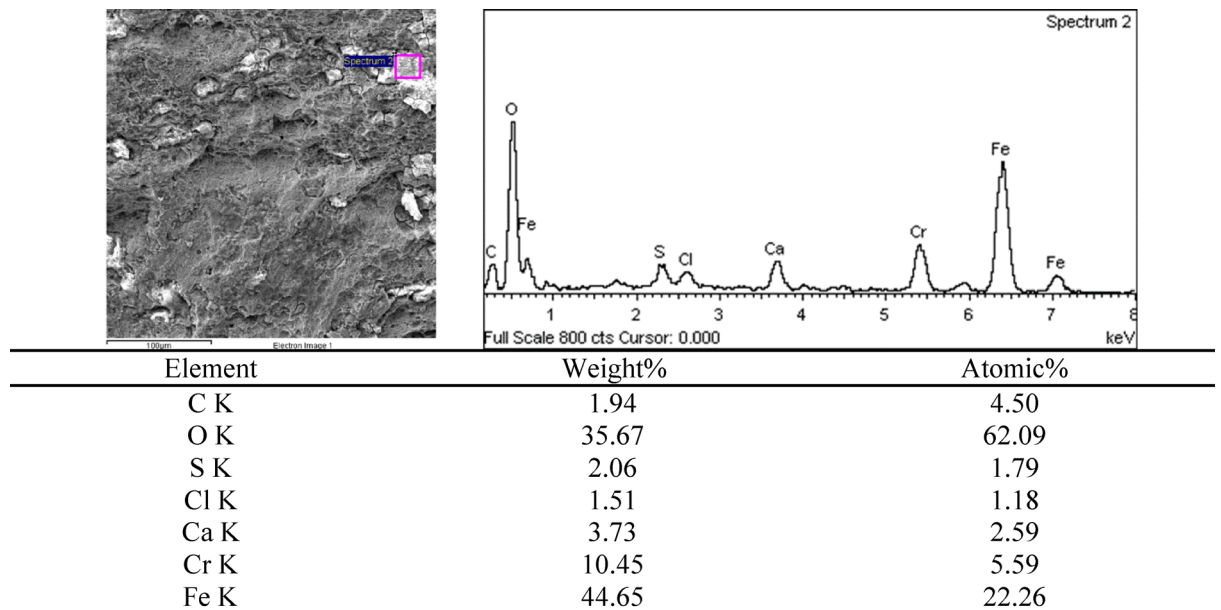


**Fig. 12.** Energy spectrum analysis results of fracture source region.

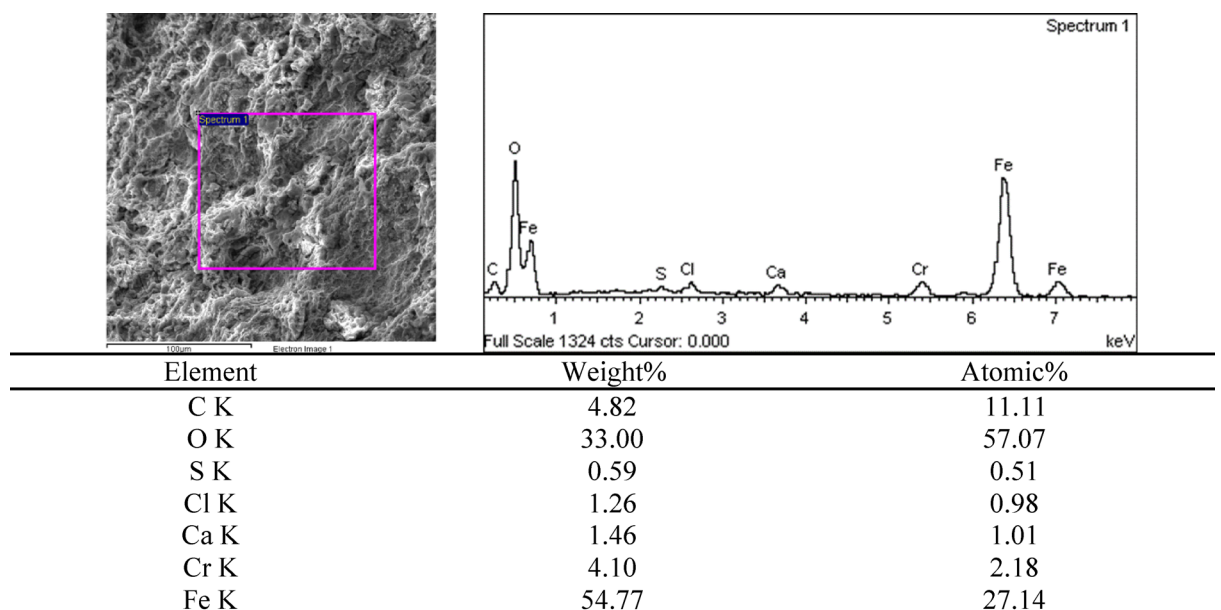


**Fig. 13.** Energy spectrum analysis results of fracture propagation zone.

as an electrolyte would accelerate the electrochemical reaction rate of the metal, making the corrosion more rapid. Thirdly, chloride would penetrate into the tip of the tiny crack, leading to further acceleration of corrosion at the crack tip thus affecting the crack expansion behavior of the metal, so that the expansion occurs under a small stress. A number of stress corrosion failures of 110 steel oil tubes in formation water environment carried out in the early days showed that 1–3% oxygen in the injected gas source significantly increases the risk of stress corrosion cracking failure of oil tubes<sup>37–40</sup>. The main reason is that oxygen dissolved in formation water activity increases, the corrosiveness of the metal is strong, which accelerates the formation water chloride ions from the oxygen corrosion region into the metal. Chloride ions accumulate at grain boundaries causing intergranular weakening, leading to chloride stress corrosion cracking of the material. At the same time, the presence of trace  $H_2S$  also accelerates the process of stress corrosion cracking.

In addition, the fractured oil tube is the 128th oil tube of the tubing column, and the depth of the well is 5860 m, and the fractured oil tube is located at 1230.04 m, which is in the upper tube section of the well's tubing column. Therefore, the oil tube was subjected to tensile load, which provided the load factor for stress



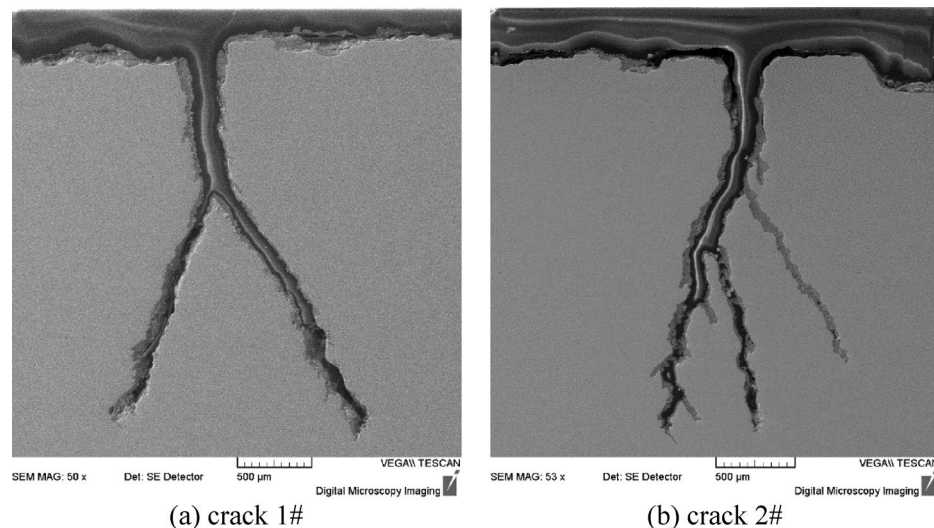


**Fig. 14.** Crack micro-morphology diagram.

corrosion cracking. What is more critical is that the well was lifted and lowered several times during the tube column lifting operation, as follows: (1) lifting the tube column up to the suspended weight of 80 t and 90 t, (the original suspended weight of the tube column was 55 t, and the self-weight of the rover was 5 t), and lowering the tube column down to the suspended weight of 53 t; (2) lifting the tube column up to the suspended weight of 92 t, and lowering the tube column down to the suspended weight of 52 t; (3) lifting the tube column up to the suspended weight of 94 t, with the packer not being unlocked; and (4) original well tubular column activity unsealing + suspension unsealing, tubular column activity range 40 t to 95 t (original suspended weight of tubular column is 55 t, traveler, square drilling rod, tap self-weight is 7 t), suspended weight of tubular column is reduced from 95 t to 20 t, continuing to lift the suspended weight of tubular column is unchanged. The suspended weight of the tube column decreased from 95 t to 20 t, indicating that the tube column was fractured. Combined with the obvious necking phenomenon in the fracture of the oil tube, it is judged that the reason for the fracture of the oil tube is that the oil tube has stress corrosion cracks, and then it is lifted up and lowered down for many times, which leads to the fracture of the oil tube.

In summary, the repaired oil tube fracture belongs to chloride stress corrosion failure. It is mainly due to the gas lift injected natural gas containing oxygen and trace hydrogen sulfide superimposed on the formation water (CaCl<sub>2</sub>) environment, forming a high stress corrosion cracking sensitivity environment, the oil tube in the service process produced stress corrosion cracking, which makes the bearing capacity of the oil tube reduced, and plastic fracture occurs under the larger axial load.

## Conclusions and suggestions

### Conclusions

Based on the in-depth analysis of the 3Cr repair tubing body fracture accident in an oil and gas well in an oilfield, the following conclusions are drawn:

- (1) The tensile strength, yield strength, Rockwell hardness and chemical composition of the oil tube material meet the requirements of the technical agreement on 3Cr low alloy steel, the metallographic organization of the oil tube is tempered austenite, with a grain size grade of 9.0, and the sum of the grades of the four types of non-metallic inclusions is not more than 2.0, and there is no abnormality in the metallographic organization of the oil tube.
- (2) A significant number of corrosion pits, with depths ranging from 0.287 to 0.785 mm, are present on the inner wall of the oil tube, and cracks are observed at the bottom of some of these pits, and the common existence of corrosion pits and cracks makes the axial bearing capacity of the oil tube decrease significantly.
- (3) The natural gas injected by gas lift contains oxygen and trace hydrogen sulfide, and the formation water is CaCl<sub>2</sub> water type, which together form a high stress corrosion cracking sensitivity environment, and the corrosion pits and stress corrosion cracks are generated in the service process of the oil tube, which reduce the bearing capacity of the oil tube, and plastic fracture occurs under a large axial load.

### Suggestions

In order to avoid the occurrence of similar tubing fracture accidents and ensure the safe production of the oilfield, the following countermeasures and improvement suggestions are put forward:

- (1) Strengthen the selection and detection of tubing materials: in the process of tubing material selection, relevant technical agreements and standards should be strictly followed to ensure that the selected materials meet the requirements for use in the harsh environment of the oilfield. At the same time, before the oil pipe

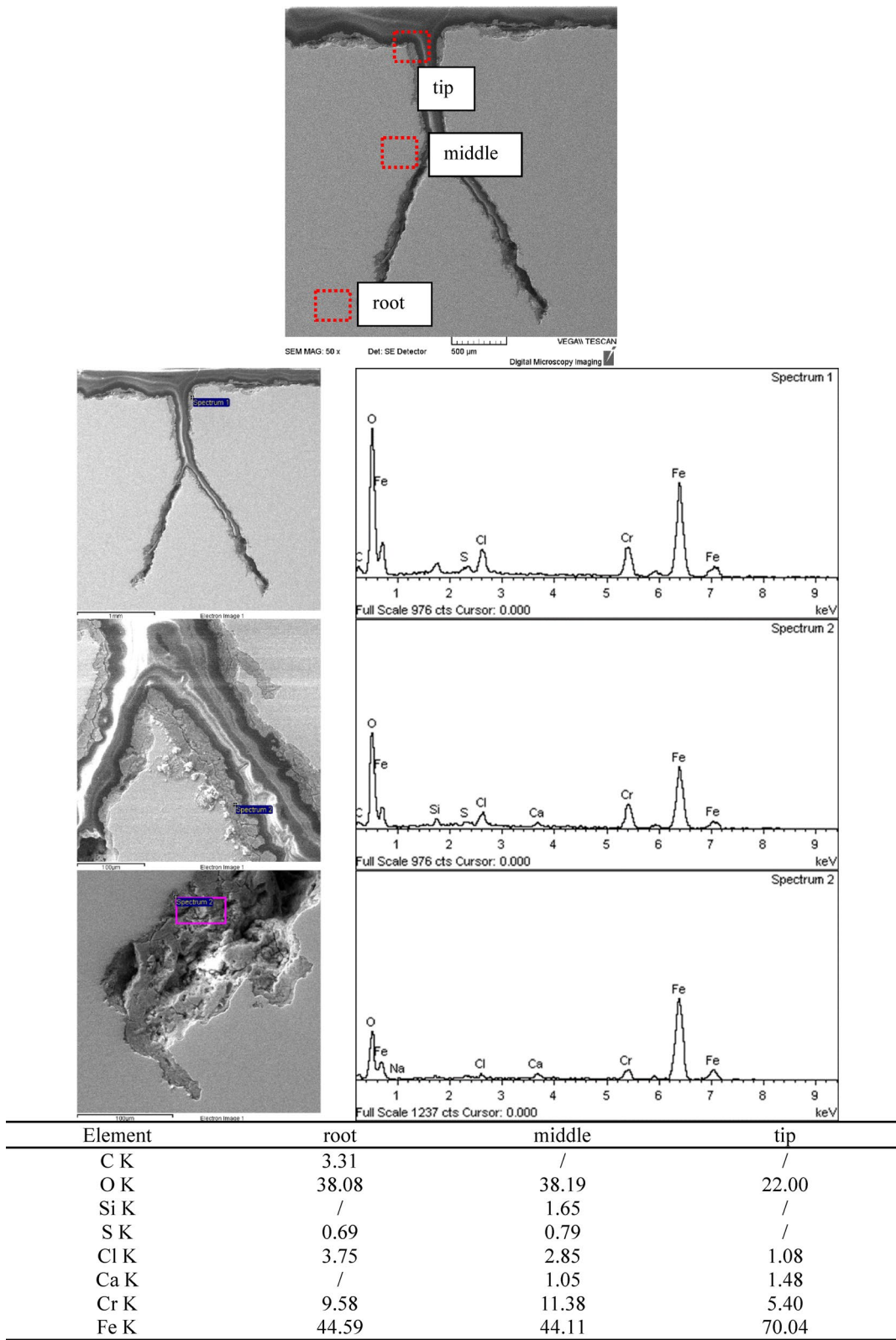


**Fig. 15.** Energy spectrum analysis results of crack 1#.

- is put into use, it should be comprehensively tested, including chemical composition analysis, mechanical property test and metallographic structure inspection, to ensure that the oil pipe quality is qualified.
- (2) Optimization of tubing repair process: for the tubing reused after repair, the repair process should be optimized to ensure the repair quality. During the repair process, special attention should be paid to the

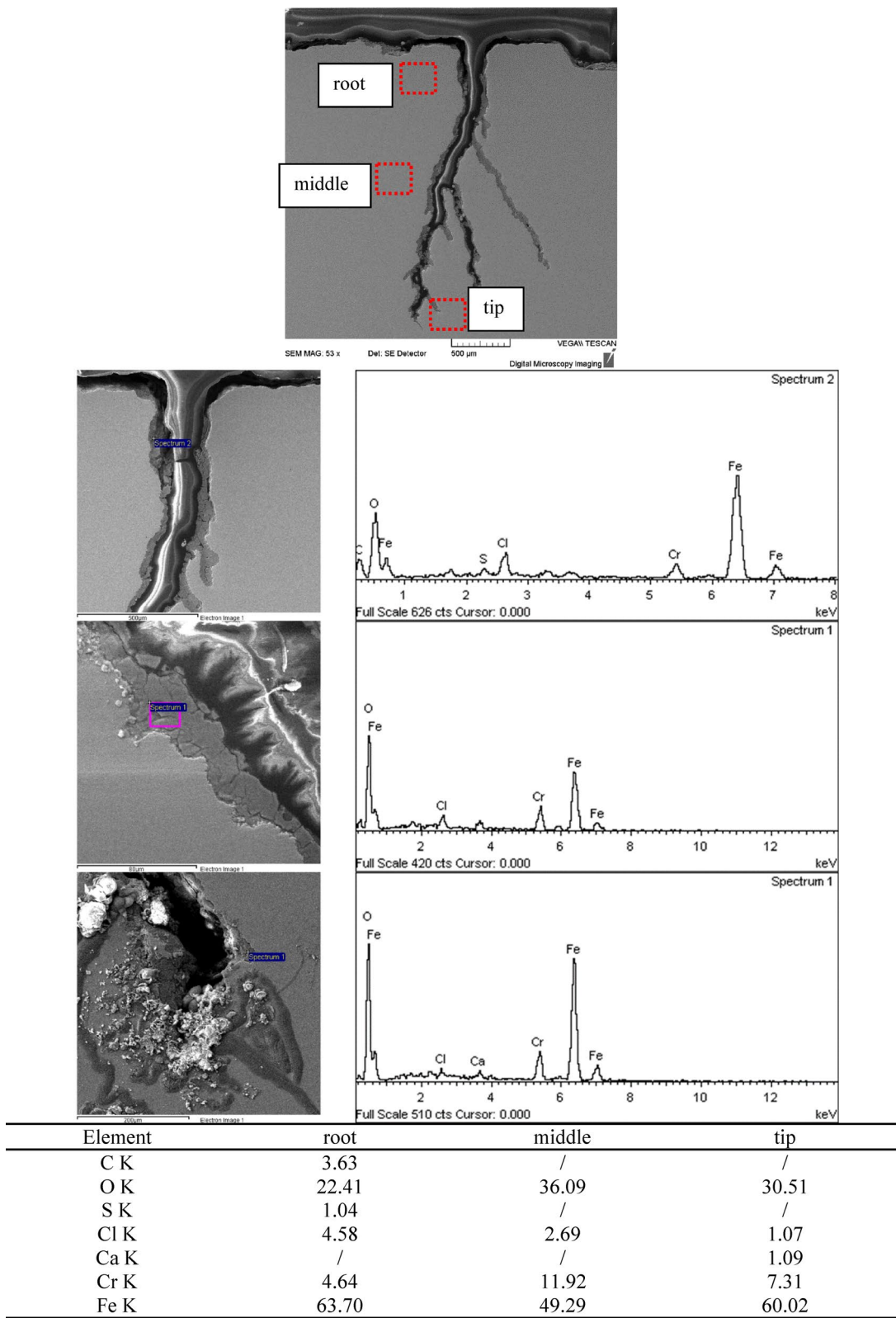
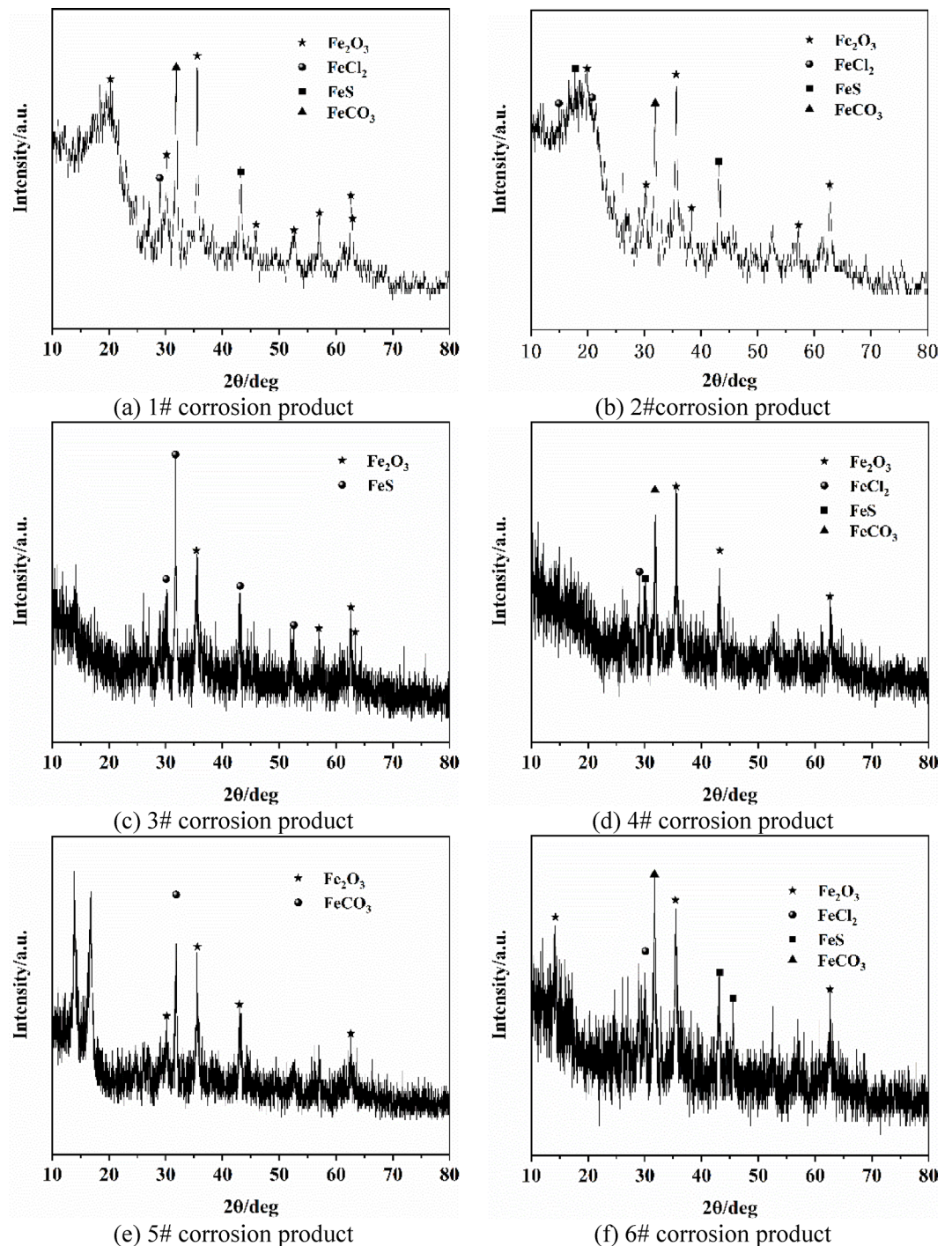


Fig. 16. Energy spectrum analysis results of crack 2#.

treatment of corrosion pits and microcracks on the inner wall of the oil pipe to avoid them becoming stress concentration points, resulting in the fracture of the oil pipe during use.

(3) Improve service environment: in view of the harsh service environment of oil pipes, measures should be taken to improve the environmental conditions and reduce the corrosion effect of corrosive media on oil





**Fig. 17.** XRD Analysis results of corrosion products on the oil tube inner surface.

pipes. For example, the natural gas injected by gas lift can be purified to remove corrosive components such as oxygen and trace hydrogen sulfide; At the same time, strengthen the monitoring and management of formation water to reduce its salinity and chloride ion content.

- (4) Strengthen monitoring and maintenance: during the service process of tubing, the monitoring and maintenance of its operation status should be strengthened. Non destructive testing technology (such as magnetic particle testing, ultrasonic testing, etc.) shall be regularly used to detect the oil pipe, and potential cracks and corrosion pits shall be found and handled in time. At the same time, the use files of oil pipes shall be established to record the use history, maintenance records, test results and other information, so as to provide the basis for the maintenance and management of oil pipes.
- (5) Improve the operation standardization: in the process of tubing lifting and lowering, the operation shall be carried out in strict accordance with the operating procedures to avoid additional stress on the tubing due



Well number	O <sub>2</sub> , %(mol/mol)	CO <sub>2</sub> , %(mol/mol)	H <sub>2</sub> S, %(mol/mol)
1#	0.3333	1.760	0.0002
2#	1.255	1.599	0.0000
3#	0.6542	2.235	0.00004
4#	1.116	1.443	0.0000
5#	0.1747	1.768	0.0003
6#	1.598	1.466	0.0000
7#	0.2176	1.717	0.00006
8#	0.2378	1.269	0.0002
9#	0.1889	1.332	0.0003
10#	1.010	1.142	0.0000

**Table 8.** Natural gas composition produced by gas lift gas source well.

to improper operation. In particular, when lifting and lowering operations are carried out, the operation speed and strength shall be controlled to avoid damage to the oil pipe.

To sum up, by strengthening the selection and detection of tubing materials, optimizing the tubing repair process, improving the service environment, strengthening the monitoring and maintenance, and improving the operation specification, the risk of tubing fracture accidents can be effectively reduced to ensure the safe production of the oilfield.

**Data availability**

The datasets used and/or analysed during the current study available from the corresponding author on reasonable request.

Received: 4 March 2025; Accepted: 3 July 2025  
Published online: 17 July 2025

**References**

1. Rizvi, S. K. A. et al. The power play of natural gas and crude oil in the move towards the financialization of the energy market. *Energy Econ.* **112**, 106131 (2022).

2. Xia, Z. et al. Cracking failure analysis on a high-frequency electric resistance welding pipe in buried fire water pipeline. *Eng. Fail. Anal.* **146**, 107072 (2023).

3. Gallego, M. et al. Influence of fluid flow in Microbiological corrosion failures in oil field injector well tubing. *Eng. Fail. Anal.* **128**, 105603 (2021).

4. Chen, S. et al. Root cause analysis of tubing and casing failures in low-temperature carbon dioxide injection well. *Eng. Fail. Anal.* **104**, 873–886 (2019).

5. Wang, Q. et al. Under-deposit corrosion of tubing served for injection and production wells of CO<sub>2</sub> flooding. *Eng. Fail. Anal.* **127**, 105540 (2021).

6. Liu, Z. et al. Failure analysis of P110 steel tubing in low-temperature annular environment of CO<sub>2</sub> flooding wells. *Eng. Fail. Anal.* **60**, 296–306 (2016).

7. Chen, X. et al. Effect of cathodic protection on corrosion of pipeline steel under disbonded coating[J]. *Corros. Sci.* **51** (9), 2242–2245 (2009).

8. Dong, C. F. et al. Effects of hydrogen-charging on the susceptibility of X100 pipeline steel to hydrogen-induced cracking[J]. *Int. J. Hydrog. Energy.* **34** (24), 9879–9884 (2009).

9. Chen, D. X. *Stress Corrosion Cracking of X80 Pipeline Steel in Simulated Alkaline Soil solution*[J] (Materials & Design, 2009).

10. Sabel, C. F. & Victor, D. G. Governing global problems under uncertainty: making bottom-up climate policy work[J]. *Clim. Change.* **144** (1), 1–13 (2017).

11. Liu, Z. Y., Li, X. G. & Cheng, Y. F. Mechanistic aspect of near-neutral pH stress corrosion cracking of pipelines under cathodic polarization[J]. *Corros. Sci.* **55** (none), 54–60 (2011).

12. Liu, Z. Y. et al. Stress corrosion cracking behavior of X70 pipe steel in an acidic soil environment[J]. *Corros. Sci.* **50** (8), 2251–2257 (2008).

13. Cui, G. G. *JixiangZhang, YuZhao, QingFu, ShunkangHan, TongZhang, ShilingWu, Yanhua. Chitosan Oligosaccharide Derivatives as Green Corrosion Inhibitors for P110 Steel in a carbon-dioxide-saturated Chloride solution*[J]203 (Scientific and Technological Aspects of Industrially Important Polysaccharides, 2019).

14. Jian, M. et al. *Corrosion Behavior of P110 Tubing Steel in the CO<sub>2</sub>-saturated Simulated Oilfield Formation Water with Element Sulfur Addition*[J] (Rare Metal Materials and Engineering, 2018).

15. Bao, M. et al. Electrochemical behavior of tensile stressed P110 steel in CO<sub>2</sub> environment[J]. *Corros. Sci.* **112** (NOV), 585–595 (2016).

16. Elgaddafi, R., Ahmed, R. & Shah, S. Modeling and experimental studies on CO<sub>2</sub>-H<sub>2</sub>S corrosion of API carbon steels under high-pressure. *J. Petroleum Sci. Eng.* **156**, 682–696 (2017).

17. Rihan, R. et al. The susceptibility of P110 downhole tubular steel to sulfide stress cracking in H<sub>2</sub>S and NaCl[J]. *J. Petrol. Sci. Eng.* **174**, 1034–1041 (2019).

18. Song, L. et al. A failure case of P110 steel tubing in CO<sub>2</sub> flooding well[J]. *Anti-Corros. Methods Mater.* **67**, 453–463 (2020).

19. Li, Y. et al. Failure analysis of the 304 stainless steel tube in a gas analyzer[J]. *Eng. Fail. Anal.* **20**, 35–42 (2012).

20. Junzhe, M. P. A. & Xiaoqing, Q. *CO<sub>2</sub>/H<sub>2</sub>S corrosion behavior of N80 steel in heterogeneous medium*[J] (Journal of Oil and Gas Technology, 2009).

21. Wang, Y. Effect of CO<sub>2</sub> partial pressure on CO<sub>2</sub>/H<sub>2</sub>S corrosion of oil tube Steels. *Adv. Mater. Res.* **962–965**, 407–410 (2004).

22. Zhu, S. D. et al. Corrosion of N80 carbon steel in oil field formation water containing CO<sub>2</sub> in the absence and presence of acetic acid[J]. *Corros. Sci.* **53** (10), p3156–3165 (2011).

23. Zhang, Z. et al. Stress corrosion crack evaluation of super 13Cr tubing in high-temperature and high-pressure gas wells. *Eng. Fail. Anal.* **95**, 263–272 (2019).
24. Elboudjaini, M. & Revie, R. W. Metallurgical factors in stress corrosion cracking (SCC) and hydrogen-induced cracking (HIC)[J]. *J. Solid State Electrochem.* **13** (7), 1091–1099 (2009).
25. Huang, F. et al. Hydrogen-induced cracking susceptibility and hydrogen trapping efficiency of different microstructure X80 pipeline steel[J]. *J. Mater. Sci.* **46**, 715–722 (2011).
26. Albarran, J. L., Martinez, L. & Lopez, H. F. Effect of heat treatment on the stress corrosion resistance of a microalloyed pipeline steel[J]. *Corros. Sci.* **41** (6), 1037–1049 (1999).
27. Barbosa, C. et al. Failure analysis of pipes used in a hydrosulfuration system of a petrochemical plant[J]. *Eng. Fail. Anal.* **13** (7), 1076–1091 (2006).
28. Xu, S. et al. Failure analysis of a carbon steel pipeline exposed to wet hydrogen sulfide environment[J]. *Eng. Fail. Anal.* **71**, 1–10 (2017).
29. Zhu, S. et al. Failure analysis of P110 tubing string in the ultra-deep oil well. *Eng. Fail. Anal.* **18** (3), 950–962 (2011).
30. Zhichao, Q. et al. Major corrosion factors in the CO<sub>2</sub> and H<sub>2</sub>S coexistent environment and the relative anti-corrosion method: taking Tazhong I gas field, Tarim basin, as an example. *Pet. Explor. Dev.* **39** (2), 256–260 (2012).
31. Lin, H. et al. Review on CO<sub>2</sub> corrosion rule of down-hole strings in Bohai oil field and current status of anticorrosion material selection [J]. *Surf. Technol.* **45**, 97–103 (2016).
32. Li, W., Zhou, Y. J. & Xue, Y. Corrosion behavior of 110S tube steel in environments of high H<sub>2</sub>S and CO<sub>2</sub> content[J]. *J. Iron. Steel Res. Int.* **19** (12), 59–65 (2012).
33. Wu, Q. et al. Corrosion behavior of low-alloy steel containing 1% chromium in CO<sub>2</sub> environments[J]. *Corros. Sci.* **75**, 400–408 (2013).
34. Xiao, R. et al. Corrosion failure cause analysis and evaluation of corrosion inhibitors of Ma Huining oil pipeline[J]. *Eng. Fail. Anal.* **68**, 113–121 (2016).
35. Subramanian, C. et al. Stress corrosion cracking of U tube heat exchanger used for low pressure steam generation in a hydrogen unit of petroleum refinery[J]. *Eng. Fail. Anal.* **137**, 106245 (2022).
36. Subramanian, C. Sulfide stress cracking of column overhead pipe to flange fitting joints in a petroleum industry[J]. *Mater. Today Commun.* **37**, 106995 (2023).
37. Luo, S. et al. Stress corrosion cracking behavior and mechanism of super 13Cr stainless steel in simulated O<sub>2</sub>/CO<sub>2</sub> containing 3.5 wt% NaCl solution[J]. *Eng. Fail. Anal.* **130**, 105748 (2021).
38. Subramanian, C., Zamindar, S. & Baneerjee, P. Oxygen corrosion of reboiler tube served in production of Dilution steam from heat exchanger of petrochemical refinery[J]. *Eng. Fail. Anal.* **164**, 108664 (2024).
39. Fan, L. et al. Failure analysis on the oxygen corrosion of the perforated screens used in a gas injection Huff and puff well[J]. *Eng. Fail. Anal.* **119**, 104984 (2021).
40. Yu, Z. et al. Investigations on the oxygen corrosion behaviors of P110 steel in a dynamic experiment simulating nitrogen injection[J]. *Mater. Corros.* **71** (8), 1375–1385 (2020).

## Acknowledgements

The work was supported by the Natural Science Basis Research Plan in Shaanxi Province of China (grant number 2023-JC-QN-0449) and the Key Core Technology Research and Development Project of CNPC (grant number 2022ZG15).

## Author contributions

Conceptualization, Jinzhi Wang and Xianren Kuang; methodology, Yan Li and Yaqin Ma; investigation, Yan Li.; resources, Jinheng Luo and Yan Long; writing—original draft preparation, Jinzhi Wang.; writing—review and editing, Xianren Kuang and Jinheng Luo. All authors have read and agreed to the published version of the manuscript.

## Declarations

## Competing interests

The authors declare no competing interests.

## Additional information

**Correspondence** and requests for materials should be addressed to J.W.

**Reprints and permissions information** is available at [www.nature.com/reprints](http://www.nature.com/reprints).

**Publisher's note** Springer Nature remains neutral with regard to jurisdictional claims in published maps and institutional affiliations.

**Open Access** This article is licensed under a Creative Commons Attribution-NonCommercial-NoDerivatives 4.0 International License, which permits any non-commercial use, sharing, distribution and reproduction in any medium or format, as long as you give appropriate credit to the original author(s) and the source, provide a link to the Creative Commons licence, and indicate if you modified the licensed material. You do not have permission under this licence to share adapted material derived from this article or parts of it. The images or other third party material in this article are included in the article's Creative Commons licence, unless indicated otherwise in a credit line to the material. If material is not included in the article's Creative Commons licence and your intended use is not permitted by statutory regulation or exceeds the permitted use, you will need to obtain permission directly from the copyright holder. To view a copy of this licence, visit <http://creativecommons.org/licenses/by-nc-nd/4.0/>.

© The Author(s) 2025